Sensors & Actuators: A. Physical 373 (2024) 115442

Contents lists available at ScienceDirect

Sensors and Actuators: A. Physical

journal homepage: www.journals.elsevier.com/sensors-and-actuators-a-physical

Laser-induced forward transfer for manufacture of graphite-based heaters on flexible substrate

Logaheswari Muniraj [a,*], Marcus Ardron [b], Juan M. Fernández-Pradas [c,d], Martí Duocastella [c,d], Pere Serra [c,d], Robert L. Reuben [e], Duncan P. Hand [a]

[a] Institute of Photonics and Quantum Sciences, Heriot-Watt University, Edinburgh EH14 4AS, UK
[b] Renishaw Plc., Research Avenue, Edinburgh EH14 4AP, UK
[c] Department of Applied Physics, Universitat de Barcelona, Martí i Franquès 1, Barcelona 08028, Spain
[d] Institute of Nanoscience and Nanotechnology (IN2UB), Universitat de Barcelona, Barcelona 08028, Spain
[e] Institute of Mechanical, Process and Energy Engineering, Heriot-Watt University, Edinburgh EH14 4AS, UK

ARTICLE INFO

Keywords:
Laser-induced forward transfer
Direct-write
Graphite heaters
Thermal management
Local heating

ABSTRACT

Flexible heaters have recently gained considerable interest owing to their ability to be integrated into a wide variety of miniaturized devices. They are used to perform thermal management, strain engineering, and even electrothermal actuation. These heaters are mainly fabricated using thin film techniques, which typically involves a multi-step lithography process that can be complex and expensive. Alternatively, wet coating methods are also employed; however, these possess several limitations when dealing with high viscosity inks. In this paper, we use a laser driven process called laser-induced forward transfer (LIFT) to fabricate graphite-based heaters on a flexible substrate. LIFT is a non-contact printing process that, unlike ink-jet printing, is nozzle-free, which makes it suitable to print any ink regardless of its viscosity. We report the first use of LIFT to print flexographic graphite ink to pattern heaters. The flexographic ink possesses high viscosity in the order of 1300–1700 mPa·s. The smallest deposit obtained using the graphite ink was 176 µm in diameter. Characterisation of the heaters shows that they can reach a wide range of temperatures at different voltage inputs. A maximum temperature of 123 °C was reached over an area of approximately 18 mm^2 at 5.2 V.

1. Introduction

Printed heater elements offer an important solution to a wide range of sensing and actuation technologies by enabling low-cost, large-area, flexible devices that manage heat transfer, providing localised and uniform heating of different surface geometries. Based on converting an electric current into thermal energy by Joule heating, micro-heaters have enabled unique advancements in the field of electronics [1], consumer appliances [2], medical diagnostic tools [3] and semiconductor manufacturing [4]. A significant amount of research is being carried out to fabricate heaters with rapid response and stable thermal management, for use in space-limited applications that require local heating and temperature control [5,6]. For instance, micro-heaters printed on insulators with large thermal expansion coefficients are used to engineer bi-axial strain in atomically thin 2D materials like MoS_2 [7]. Such micro-heaters are fabricated using a multi-step lithography process that is highly complex and expensive. Alternatively, micro filament heaters fabricated using direct-write techniques such as electro-hydrodynamic printing have been used in soft robotics, where the thermal energy provided by the heaters drives electro-thermal actuators to provide bending, which can be utilised for mechanical functions including gripping, moving, and releasing objects [8]. Although this technique is preferred for producing micro-structures with high resolution, the quality of the print is highly dependent on atmospheric conditions such as temperature and humidity. Also, the high voltage requirements of this technique can affect its applicability to many substrates and inks, restricting large-scale manufacturing.

Other fabrication technologies include wet-coating techniques such as spray coating and rod coating to manufacture carbon nanotube-based transparent micro-heaters [9]. Such film heaters owe their rapid thermal response to excellent thermal and electrical properties, and they find large-scale applications, for example in vehicle windscreen defrosters. Screen printing is extensively used for large-scale manufacturing of stretchable heaters in wearable electronics with high throughput and

* Corresponding author.
E-mail address: llm5@hw.ac.uk (L. Muniraj).

https://doi.org/10.1016/j.sna.2024.115442
Received 27 September 2023; Received in revised form 13 April 2024; Accepted 30 April 2024
Available online 3 May 2024

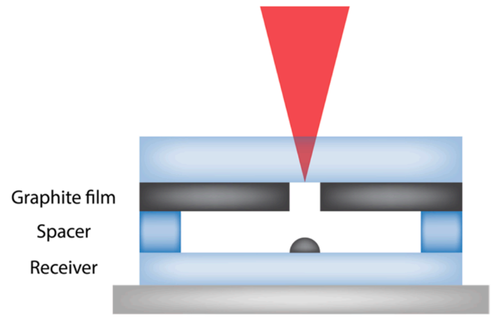

Fig. 1. Illustration of the LIFT process depositing graphite into a microscope slide receiver.

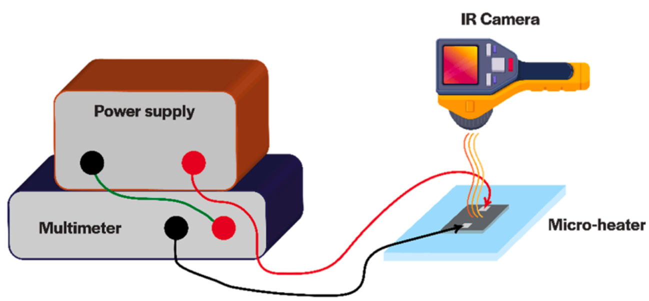

Fig. 2. Schematic representation of Joule heating setup. The power supply, sample and the multimeter are connected in series. The voltage is varied using the power supply, and the digital multimeter measures the consequent current. The IR camera measures the 2D temperature map of the sample.

low production costs. However, this requires close control of the ink's rheological properties as these strongly impact the screen-printing process itself, as wells as the properties of the final printed surface [10]. Ink-jet printing is particularly attractive in printed electronics due to its ability to print conductive inks such as silver nanowires [11], graphene [12], and graphene-oxide [13] onto flexible substrates and it is compatible with roll-to-roll (R2R) manufacturing processes. Ink-jet printing also offers high resolution but can only handle low-viscosity inks with low solid content to eliminate any potential nozzle clogging issues [14] thus preventing many functional inks from being deposited in this way. Therefore, there is a high demand for a technique that is capable of printing heaters from high viscosity inks.

A potential solution to address this gap is Laser-induced Forward Transfer (LIFT) [15]. LIFT is a non-contact printing process that uses laser pulses to eject material from a layer (the material to be printed) on a donor substrate to another (receiver) substrate, as shown in Fig. 1. Essentially, it is a drop-by-drop deposition technique that is entirely nozzle-free and can print a wide variety of materials including metals [16], biological structures [17], and functional inks [18]. LIFT of solid thin film was reported by Bohandy et al. [19] in 1986 by printing copper and silver lines. However, this process is not suitable for printing delicate materials that are prone to decomposition. Pique et al. [20] proposed a modified LIFT process called matrix-assisted pulsed-laser evaporation-direct write (MAPLE-DW) in which the donor material is embedded inside a matrix of a polymer that is highly absorbent of the laser radiation. Upon irradiation, the polymer decomposes depositing the material of interest on the receiver substrate. Following this several research groups have reported various studies about LIFT of inks based on the mechanisms of fluid ejection [21], droplet formation [22], role of laser parameters [23,24]and the properties of the liquid [25,26]. LIFT is also applicable to a large variety of substrates and provides high resolution without inherent ink viscosity restrictions (viscosities from 1-100 Pa·s have been demonstrated with LIFT) [27].

LIFT has been used to fabricate functional devices; for example, Sopena et al. [28] reported the fabrication of a radio-frequency inductor by transferring layers of silver interconnects onto paper. Also, LIFT-printed thick film electrodes ($LiCoO_2$ – cathode and carbon – anode) for Li-ion micro-batteries have been shown to exhibit 10 times higher discharge capacity, power, and energy densities than sputter deposition techniques [29], attributable to the high porosity of the laser-printed electrodes. Overall, LIFT has proven to be a highly versatile process that can print 3D patterns without the use of any screens or masks, thus providing the flexibility to change patterns dynamically in-process. Still, the printing of heaters by LIFT has not yet been reported.

In this paper, we demonstrate the fabrication of graphite heaters using a commercially available flexographic ink as an illustration of the feasibility of using LIFT to print high viscosity, cost-effective inks. We studied the effect of multiple printings by investigating the morphology and electrical resistance of the printed graphite heaters.

2. Methods

A Q-switched Ytterbium-doped fiber laser (Rofin F20 Varia) operating at 1064 nm with a maximum average power of 20 W was used for the LIFT process. The process parameters such as the pulse energy (5–800 μJ), pulse length (4–200 ns) and repetition rate (2 kHz-1 MHz) can be varied using the Visual Laser Marker software. The output beam was directed onto a 2-axis galvanometric scanner which was used to position the beam on the donor substrate. The laser beam has a Gaussian intensity profile and was focused to a diameter of 40 μm using an f-theta lens (f = 100 mm) that was placed at the output of the galvanometric scanner.

A commercially available conductive graphite ink (code 901970, Sigma-Aldrich), which has a nominal viscosity of 1300–1700 mPa·s was used as the donor material. Conventional microscope slide glass substrates (75 × 25 × 1 mm) were used for LIFT trials. 250 μm thick Polyethylene terephthalate (PET) (GoodFellow Cambridge Limited, Huntingdon, UK) was used as a flexible substrate for the resistive heating application trials. Conductive silver paint (RS Components) was used to make electrical connections on non-solderable surfaces.

2.1. Donor film preparation

The donor graphite ink was deposited manually due to its high viscosity. Firstly, the glass substrate was cleaned thoroughly with soap and rinsed with ethanol and distilled water. A 50 μm deep miniature reservoir was then created on the substrate by using 3 M Scotch Magic™ tape (invisible matt tape) as the reservoir walls. The graphite ink was placed within this reservoir and spread using a doctor blade [30]. The Scotch tape ensured that the donor film was of uniform thickness (~50 μm).

2.2. LIFT setup

A schematic diagram of the LIFT setup is shown in Fig. 1. The receiver substrate was held in place using a vacuum chuck and aligned perpendicularly to the laser beam. Since stable jet formation is expected when the donor film thickness matches the distance between the substrates for high solid content inks [31]. A gap of 50 μm was maintained in between the donor and receiver substrates using an invisible matt tape.

The laser beam was focused on the interface between the transparent donor substrate and the liquid graphite layer. As the laser pulse is incident on the surface, the energy absorbed by the donor film leads to the formation of a vapour bubble. The high pressure inside the bubble leads to the ejection of a jet, which continues to advance towards the receiver substrate depositing a liquid droplet [32]. The size of the deposits can be varied by changing the process parameters such as beam diameter, laser pulse energy, and thickness of the donor film.

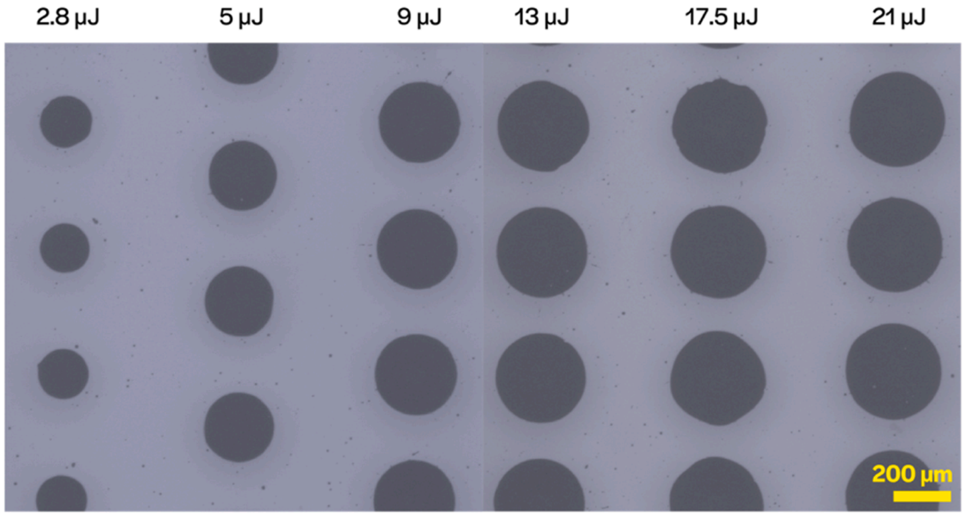

Fig. 3. Graphite deposits printed at increasing pulse energies.

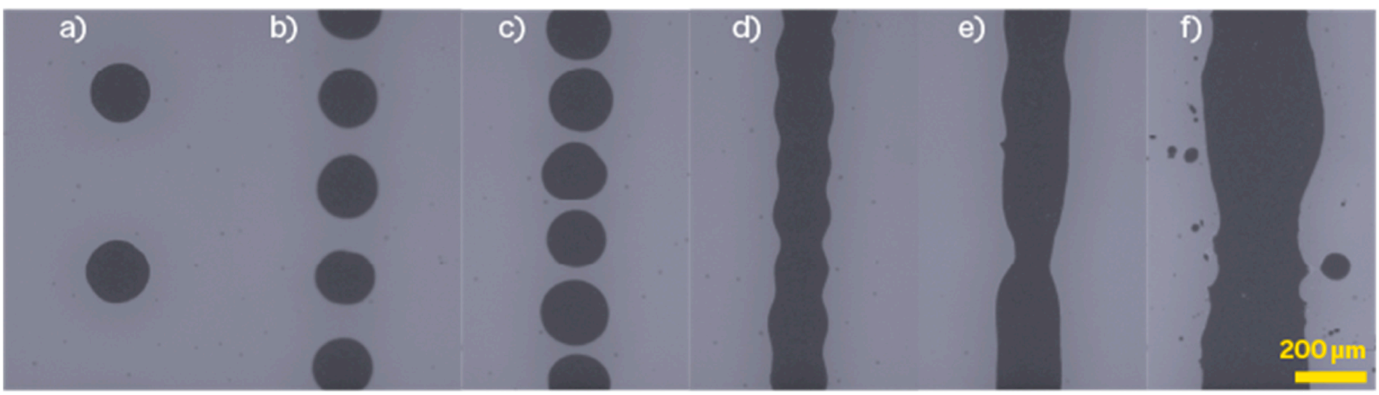

Fig. 4. Graphite deposits printed at decreasing scan speeds: a) 1000 mm/s, b) 500 mm/s, c) 400 mm/s, d) 300 mm/s, e) 200 mm/s, f) 100 mm/s.

2.3. Curing

After printing, the deposited graphite ink was cured at 90 °C for 5 minutes in a conventional oven to enhance its functionality. Silver electrodes were manually added using a paintbrush and left to air dry for 48 hours.

2.4. Characterisation

The morphology of the deposited layers was characterised using a conventional optical microscope (model AX10, Carl Zeiss), scanning electron microscope (SEM) (Vega, TESCAN) and a confocal optical microscope (S Neox, Sensofar). The resistance of the heaters was measured using a DC power supply (Aim-TTi EL302-USB Bench Power Supply (0–30 V, 2 A)) to vary the voltage and recording the consequent current using a digital multimeter (34401a, Hewlett Packard), as shown in Fig. 2. A 2D temperature map of the upper surface of the samples was measured using a thermal imaging camera (i7, FLIR).

3. Results

3.1. Fabrication of graphite heaters by laser-induced forward transfer

First, we optimized conditions for printing high viscosity graphite ink for fabricating the heaters by transferring individual deposits. A range of pulse energies from 2.8 µJ (the minimum pulse energy observed to lead to transfer) to 21 µJ, for a fixed 4 ns pulse length, was used to LIFT an array of graphite deposits. The scanning speed and pulse repetition rate were set to 1000 mm/s and 2 kHz, respectively, which meant that a separate deposited spot was obtained for each laser pulse, as shown in Fig. 3.

As can be seen, the diameter of the deposits increases with laser pulse energy, a phenomenon generally observed in LIFT of liquids [18]. A minimum diameter of 176 µm was measured for the deposit printed at 2.8 µJ, which is the transfer threshold, below which no deposits could be printed. Most inks exhibit a narrow pulse energy window for well-defined deposits, beyond which the jet becomes unstable due to excessive mechanical stresses leading to non-uniform deposits [33]. The graphite ink maintains uniform jetting even at high energies due to its high viscosity [34]; with minimal debris around the deposits, without compromising its functionality in terms of resistance.

In LIFT of inks, the transferred ink remains in its liquid state until cured. Therefore, when printed close enough to each other, the deposited liquid droplets coalesce, forming a line. To investigate the influence of overlap, a range of scan speeds were tested, from 1000 mm/s to 100 mm/s, for a fixed pulse energy of 2.8 µJ. Fig. 4 shows the evolution of droplets to lines at different overlaps. As coalescence begins, (Fig. 4d), the droplets form wavy lines of maximum width equal to the diameter of the individual droplets. This could lead to an unfavourable change in cross-sectional area affecting the resistance for conductive inks. Beyond 300 mm/s (Fig. 4d) the width of the printed lines increases with the degree of overlap. If the scan speed is too low (e.g. Figs. 4e and 4f), the short distance between the droplets impacts the vaporisation bubble resulting in an unstable jet [35]. This leads to break-up of the droplets

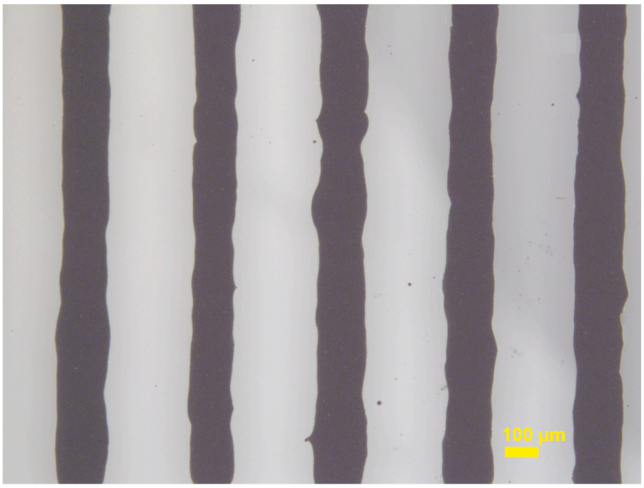

Fig. 5. Graphite lines printed at 3.5 µJ and scanning speed of 250 mm/s.

during transfer and hence produce scattered satellite deposits or broken lines with varying non-uniform widths. For this pulse energy, the optimal scan speed is clearly between 300 mm/s (Fig. 4d) and 200 mm/s (Fig. 4e).

Further optimisation demonstrated that the most uniform lines are obtained at a scan speed and pulse energy of 250 mm/s and 3.5 µJ, respectively, with examples shown in Fig. 5. The average width of these lines is 150 µm, with a maximum width of 180 µm and a minimum of 115 µm.

Using the optimised parameters, square graphite heaters of varying sizes (5 × 5 mm^2 down to 1 × 1 mm^2) were printed on a glass substrate (Fig. 6) and cured. To enhance the thickness of the graphite heater and hence reduce sheet resistance, multiple layers were printed consecutively on top of each other. A fresh donor film was used for each printed layer.

Fig. 7 shows the SEM image of a 5 × 5 mm^2 graphite square using a single, double and triple printings. The surface of all the printings looks comparable, due to the high graphite content in the ink. However, with additional layers the graphite particles are seen to form larger clusters.

Fig. 8 shows the cross-sectional view of a 5 × 5 mm^2 graphite square using a single, double and triple printings on glass substrate. There are no significant voids in between the layers and with the glass substrate.

Example cross-sectional profiles of 1 × 1 mm^2, 2 × 2 mm^2 and 3 × 3 mm^2 graphite squares printed onto a glass substrate are shown in Fig. 9. The average thickness of a single print was 9.9 ± 2.1 µm, a double print 16 ± 1.0 µm, and a triple print 24.6 ± 0.8 µm. With additional layers the surface roughness is slightly improved, from an average roughness of 0.39 µm (one print) to 0.29 µm (three prints). The homogeneity observed in multiple printings is attributed to the fact that each stacked layer fills up any voids or defects left by the previous layer [36]. Multiple over-printings, therefore, not only help in decreasing the sheet resistance but also reduce any printing irregularities and flatten them. This is helpful to maintain uniform resistance and hence uniform heating throughout the heater. Furthermore, the thickness of the LIFT printed layer (tens of µm) is comparable to screen-printing and larger than those obtained via inkjet printing (<1 µm), providing a unique method to produce high-aspect ratio patterns.

3.2. Electrical characterization of the printed heaters

Next, we characterized the electrical properties of the printed heaters. Assuming that the material properties are uniform, the electrical resistance as a function of the resistivity of the material (ρ), length (l), and cross-sectional area (A) of the printed square is given by,

$$R = \rho \frac{l}{A} = \rho \frac{l}{wt}, \tag{3}$$

where w is the width of the square and t is the thickness.

Given that the printed heaters are square (i.e. $w=l$), R should be the same for all sizes of square for a given thickness, i.e. the only variation expected is that due to the number of printed layers. The resistance of

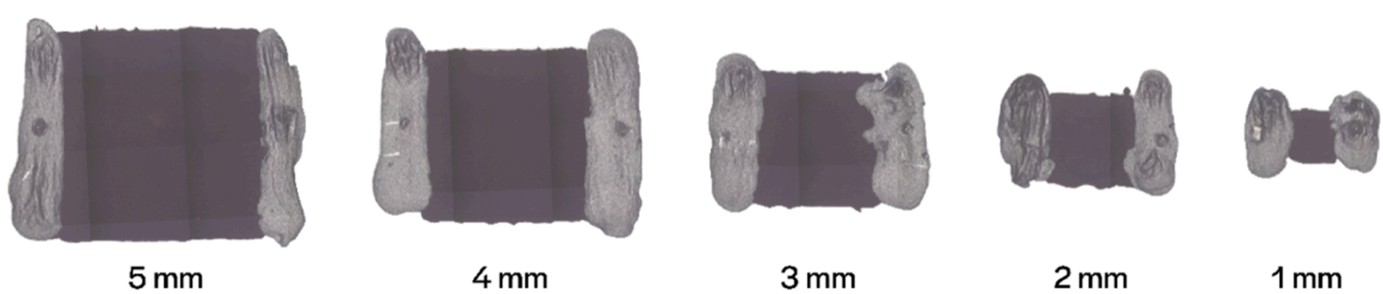

Fig. 6. Microscope image of graphite deposits of varying sizes (5 × 5 mm^2 to 1 × 1 mm^2). Silver electrodes are manually added for further characterizations.

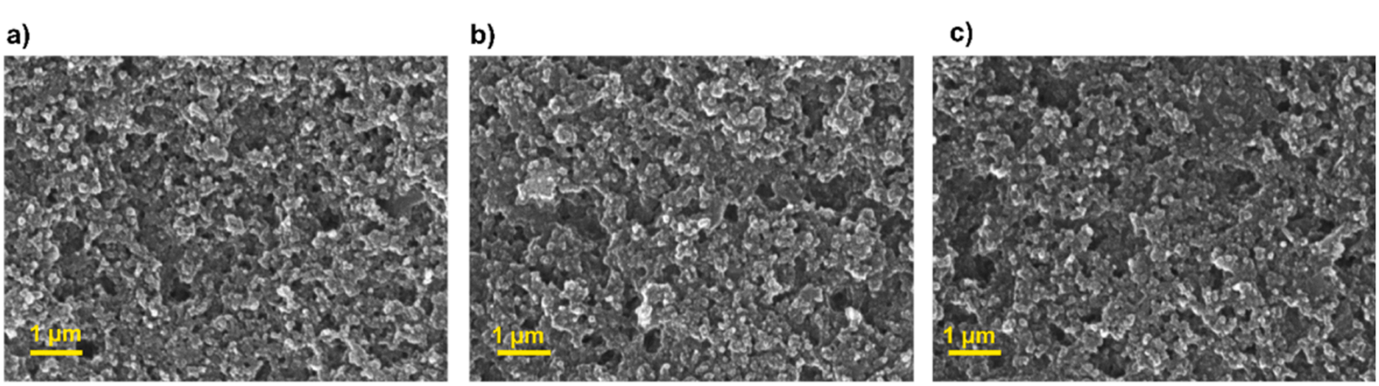

Fig. 7. SEM image of a 5 × 5 mm^2 graphite square using a a) single, b) double and c) triple printings.

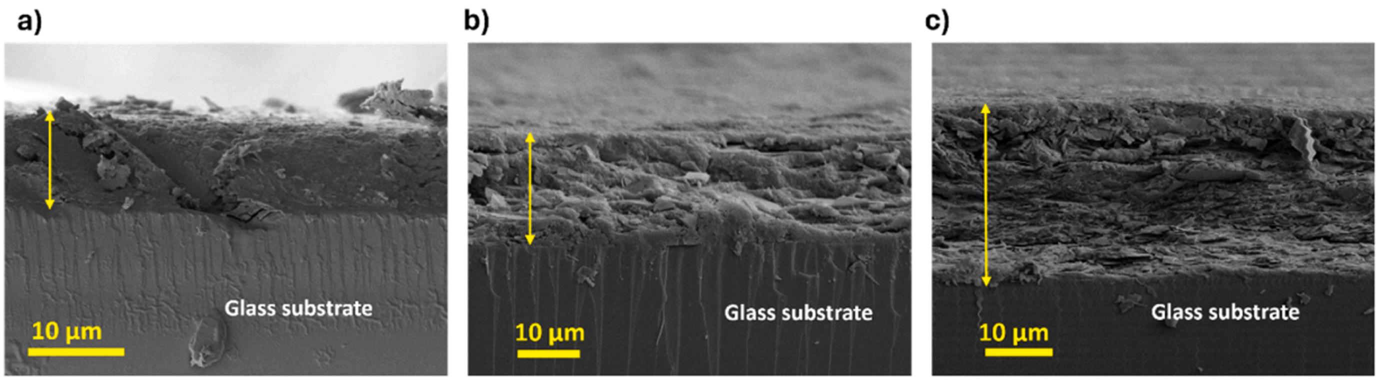

Fig. 8. SEM image of the cross-sections of 5 × 5 mm^2 graphite square using a) single, b) double and c) triple printings. Arrows denote the LIFT deposited layers.

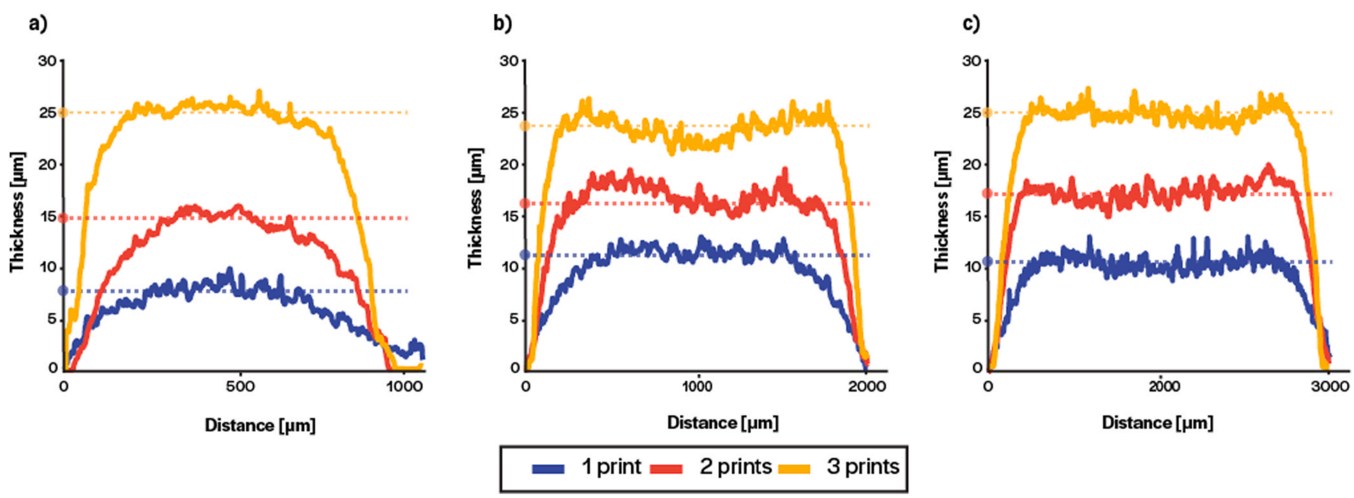

Fig. 9. Cross-sectional profile of a) 1 × 1 mm^2, b) 2 × 2 mm^2, and c) 3 × 3 mm^2 graphite deposits for single, double, and triple printings.

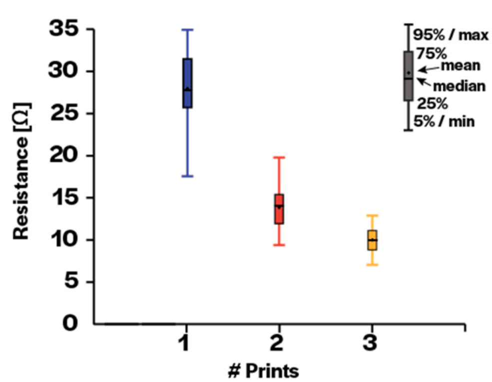

Fig. 10. Plot of electrical resistance as a function of number of printings. Box plot bars represents the distribution of resistance obtained using 12 squares of various sizes for print 1, print 2 and print 3 (a total of 36 graphite heaters).

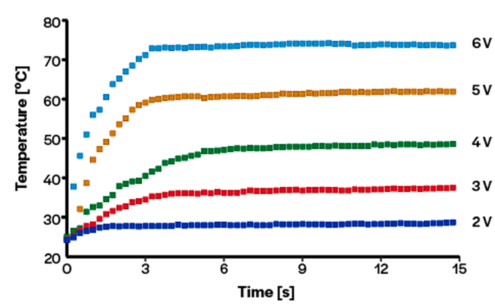

Fig. 11. Temperature profile of 18 mm^2 graphite heater (48.6 Ω). a) Time-dependent characteristic of the heater at different voltage inputs.

the squares measured as a function of the different number of printings is plotted in Fig. 10.

As expected, the resistance decreases with increasing thicknesses. The surface properties of the substrate along with the morphology of the ink determine the thickness and uniformity of the printed layer [37], as indicated by the results plotted in Fig. 8. In particular, the interquartile range for a single print is considerably higher than for multiple printings. This can be attributed to the inhomogeneous surface distribution of the deposited droplets during the printing process as fresh donor films are used for every print. The variation in thickness of the donor films affects the thickness of the deposits, thus leading to changes in resistance of the printed squares. This effect, however, gets averaged out with multiple printings lowering the uncertainty. The average resistivity of graphite heaters obtained by one print is 0.026 ± 0.004 Ω·cm, two prints is 0.025 ± 0.004 Ω·cm and three prints is 0.024 ± 0.002 Ω·cm. These values are comparable to the values quoted in literature for high viscosity inks [38]. Overall, the resistance values can be adjusted by adding layers demonstrating the ability of LIFT to control the surface conductivity of the deposited structures.

3.3. Heater performance

Micro-heaters are used in a wide variety of applications depending

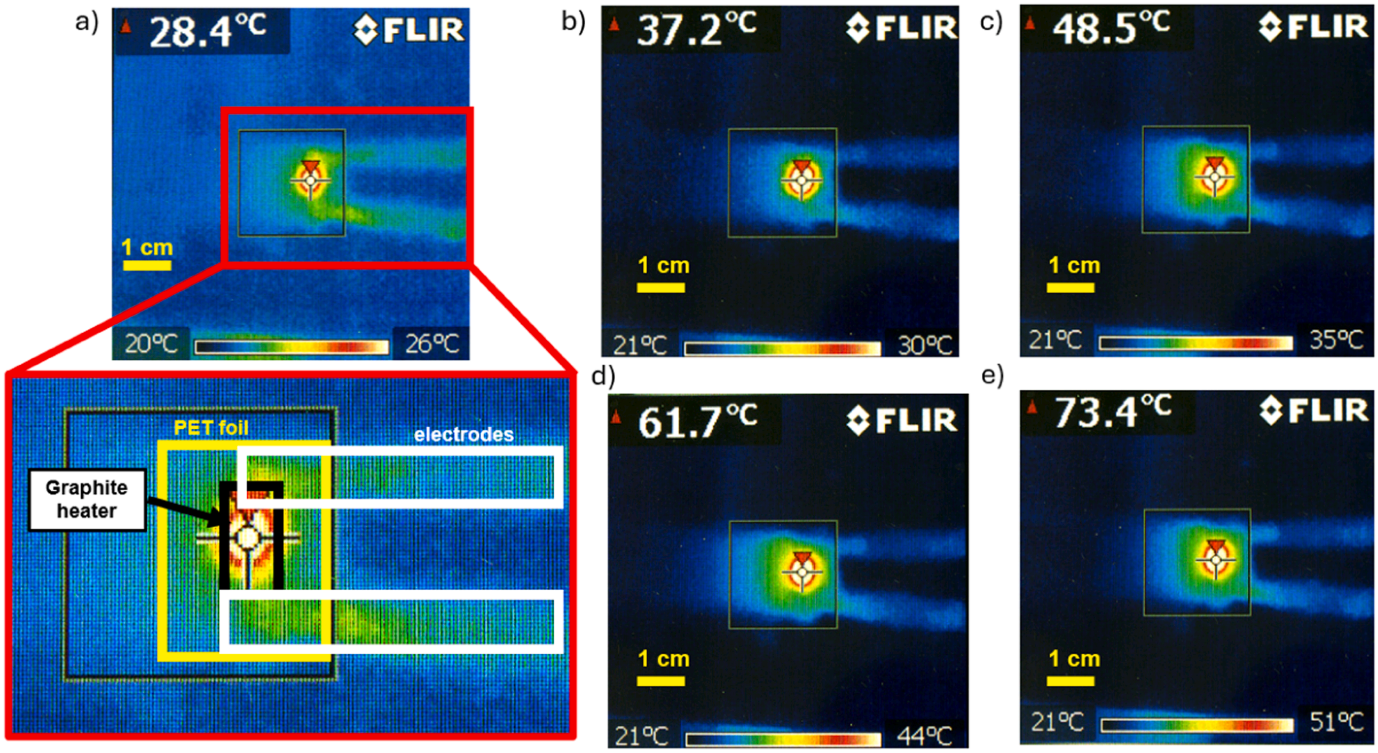

Fig. 12. Thermal image of the surface temperature of a 18 mm^2 graphite heater printed on PET foil with a resistance of 48.6 Ω at a) 2 V, b) 3 V, c) 4 V, d) 5 V and e) 6 V. Inset shows an enlarged thermal image marking the size of the heater, substrate, and electrodes. The big square on the images denotes the region of interest and the marker is at the region with maximum temperature.

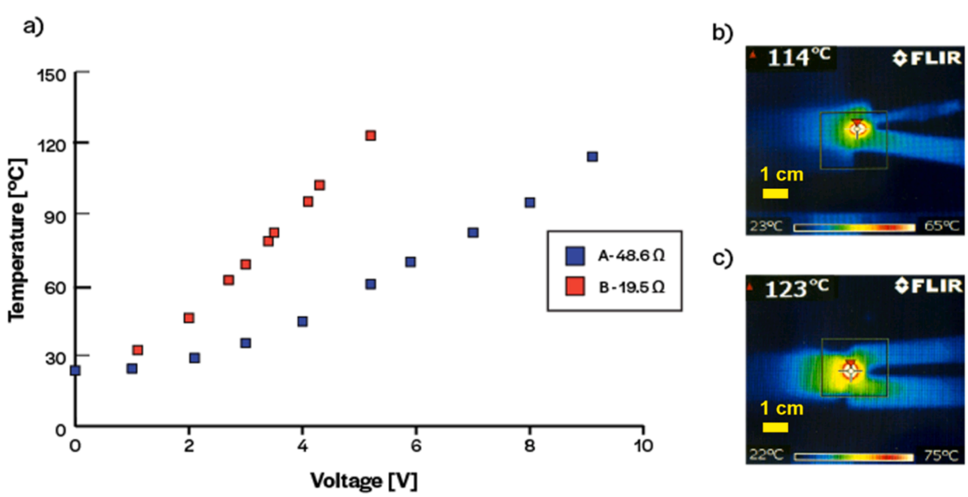

Fig. 13. a) Maximum temperature reached by the heater as a function of different voltage inputs for 2 different heaters of size 18 mm^2 with electrical resistances 48.6 Ω and 19.5 Ω, respectively. Thermal image of the maximum surface temperature reached by the heater with an electrical resistance of b) 42.6 Ω and c) 19.5 Ω. The big square on the images denotes the region of interest and the marker is at the region with maximum temperature.

on their size, response rate, and design. They are typically required to provide a homogeneous temperature across the heater surface. Using a substrate with low thermal conductivity and high specific heat capacity can directly lower the heat loss due to diffusion and thereby reduce the response time and overall functionality of the heater. Therefore, we evaluated the heater performance by printing them onto PET foil using the same laser parameters as optimised with the glass substrate (scan speed and pulse energy of 250 mm/s and 3.5 μJ, respectively). However, it is worth noting that the temperature distribution and heat dissipation would, in practice, depend on the thermal conductivity and heat capacity of the base substrate on which the PET is placed.

A sample heater of size 6 × 3 × 0.012 mm (resistance 48.6 Ω) printed onto a PET foil of thickness 250 μm was placed on top of a stainless-steel block of dimensions 55 × 14 × 1.5 mm. Different voltage inputs (varied from 2–6 V) were applied to the heater and its surface temperature was measured over a period of 60 s using a thermal camera. The temperature profiles obtained for the heater are shown in Fig. 11. As expected, for a given applied voltage, the temperature of the heater keeps increasing until a steady state temperature is reached, typically after 10–12 s, and this final temperature increases monotonically with applied voltage. Fig. 12 shows the thermal images recorded by the IR camera at different voltages. The maximum

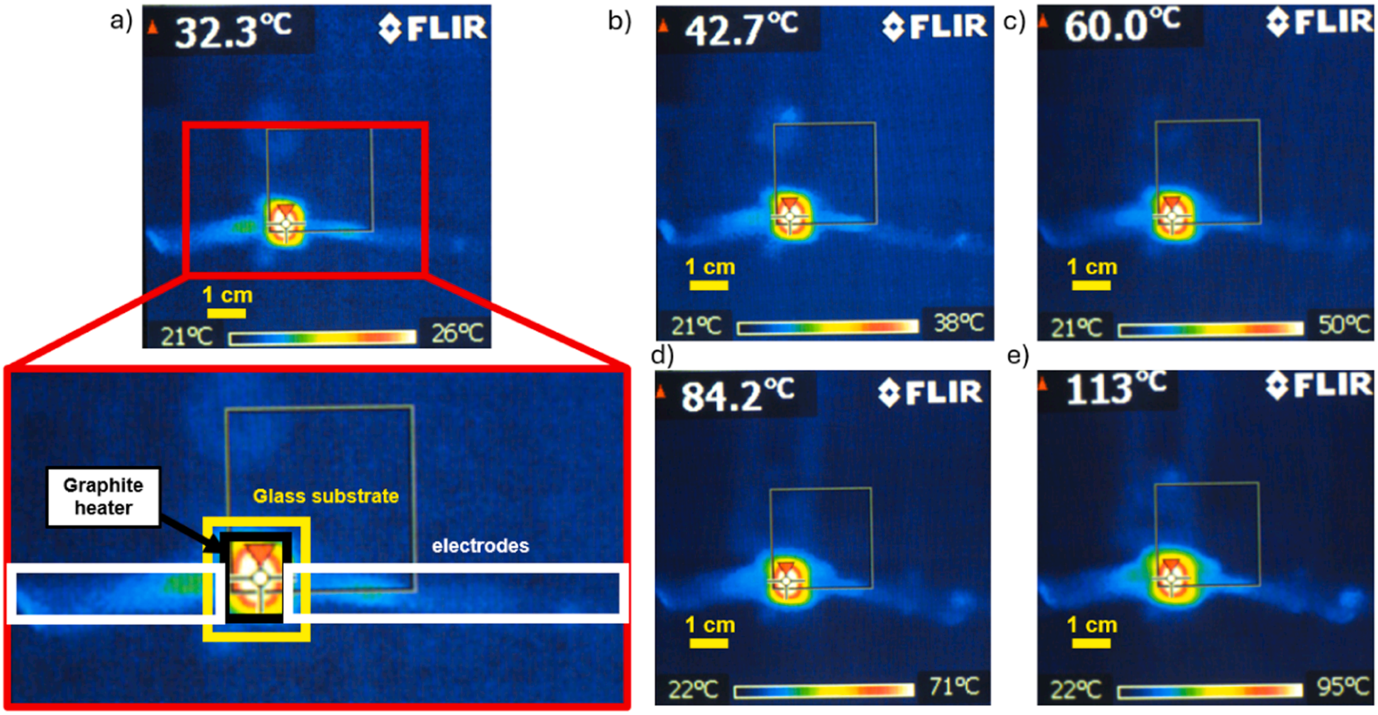

Fig. 14. Thermal images of the surface temperature of a 25 mm^2 graphite heater printed on glass with a resistance of 40.2 Ω at a) 2 V, b) 3 V, c) 4 V, d) 5 V and e) 6 V. Inset shows an enlarged thermal image marking the size of the heater, substrate, and electrodes. The big square on the images denotes the region of interest and the marker is at the region with maximum temperature.

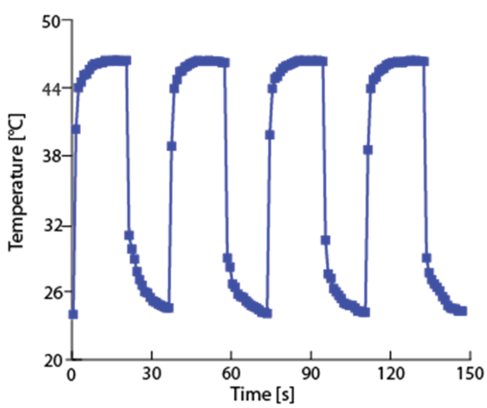

Fig. 15. Cyclic heating performance of heater A with resistance 48.6 Ω (18 mm^2) at 4 V.

temperature is indicated at the top left corner of the thermal images. As can be seen from the thermal images, the PET foil provides good heat confinement for the heater due to its low thermal conductivity. There is, however, some heat dissipation at the electrical connections which can be observed at the right-hand side of the heater, and hence the maximum temperature was recorded at the centre of the heater geometry. The heat dissipation surrounding the heater increases at higher voltages, indicating the thermal losses, Fig. 12, caused by thermal conduction, convection, and radiation.

Fig. 13 shows the voltage dependent temperature profiles of two heaters with different electrical resistances; heater A (18 mm^2) deposited with a single LIFT print and heater B (18 mm^2) deposited using two LIFT prints leading to resistances of 48.6 Ω and 19.5 Ω, respectively.

The maximum steady-state temperature reached by heater A at 9.1 V (928 mW) was 114 °C and heater B at 5.2 V (608 mW) was 123 °C. Under the application of same voltage (5.2 V), the maximum steady state temperature rise reached by heater B is two times the temperature reached by heater A. As shown in Fig. 13 b) and c), the square tracker from the camera display highlights the maximum temperature within the area of interest. This is shown to be at the centre of the heater in both the cases. There is, however, an increased amount of heat dissipation at the edges and the electrical connections of heater B as at higher temperatures one can expect higher heat accumulation and thermal losses.

This experiment was limited because, beyond 150 °C, the PET foil starts to get irreversibly deformed showing signs of damage around the heater. Performing the same experiment (varying voltage (2–6 V) and measuring temperature) with a heater printed on glass, higher temperatures can be reached (Fig. 14). A maximum of 213 °C was recorded at 9 V. Beyond this, the glass broke proving that the graphite heater can handle higher temperatures.

The cyclic electrical heating performance of heater A at 4 V is shown in Fig. 15. Upon periodically switching the voltage ON and OFF, we can observe that the heater is able to repeatedly reach the same temperatures. The similarity in the heating patterns demonstrates the stability and repeatability of the heaters. Fig. 16 shows the heating performance of the heater when subjected to one-off mechanical bending. Upon deformation, the heater reaches higher temperature due to the decrease in cross-sectional area. Using the related photos and IR images we can confirm that the heater functions despite deformations without a significant change in resistance.

With our basic design, we have demonstrated the stability, repeatability, and flexibility of the printed graphite 3D heater using LIFT, showcasing its ability to be used on various surfaces and materials. Depending on the thermal properties of the base substrate, the temperature distribution will vary. However, the geometry of the heater can be tailored to customise heat distribution for specific applications.

4. Conclusions

LIFT can be successfully used to fabricate graphite-based heaters. We have demonstrated the use of LIFT for printing 3D patterns of varying

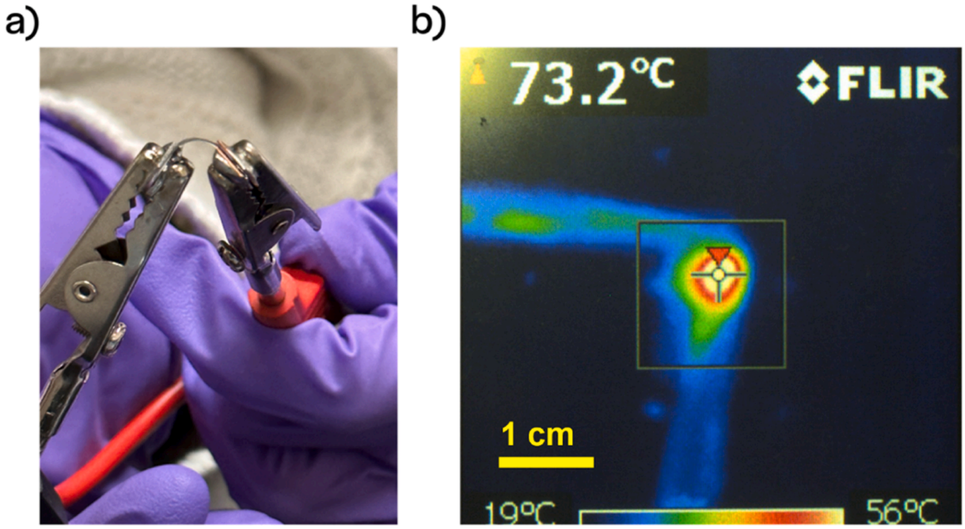

Fig. 16. a) Mechanical deformation induced on heater A. b) Temperature measured during the deformation using an IR camera. The big square on the images denotes the region of interest and the marker is at the region with maximum temperature.

resistances using a cost-effective flexographic graphite ink. The size of the heaters can scale from the diameter of a single deposit (176 μm) to larger areas, making them an attractive alternative to conventional printing techniques. The heater performance of the fabricated graphite structures on PET foil was investigated. A thermal equilibrium temperature of 123 °C was obtained with 5.2 V, limited only by the PET foil substrate.

The versatility of LIFT will enable integration of the heaters into many functional devices where miniature resistive elements are often essential components.

CRediT authorship contribution statement

Duncan P Hand: Writing – review & editing, Supervision, Conceptualization. **Robert L Reuben:** Writing – review & editing, Supervision, Conceptualization. **Juan M Fernández-Pradas:** Writing – review & editing, Supervision, Investigation. **Marcus Ardron:** Supervision, Conceptualization. **Pere Serra:** Writing – review & editing, Supervision. **Martí Duocastella:** Writing – review & editing, Supervision, Conceptualization. **Logaheswari Muniraj:** Writing – review & editing, Writing – original draft, Methodology, Investigation, Formal analysis, Data curation, Conceptualization.

Declaration of Competing Interest

The authors declare that they have no known competing financial interests/personal relationships that could have appeared to influence the work reported in this paper.

Data availability

Data will be made available on request.

Acknowledgements

This research was supported by The Professor Julian Jones Prize for funding (travel scholarship for L Muniraj) to support the joint work at the University of Barcelona. Also supported by the National Manufacturing Institute Scotland (NMIS) for partial funding of the PhD scholarship (for L Muniraj). Drs. Fernández-Pradas, Duocastella and Serra acknowledge financial support from MCIN/ AEI/10.13039/ 501100011033/ (project PID2020–112669 GB-I00). L Muniraj would like to thank Neil Ross for the SEM images and Mark McDonald for proofreading the article.

References

[1] K.Y. Mitra, M. Polomoshnov, C. Martínez-Domingo, D. Mitra, E. Ramon, R. R. Baumann, Fully inkjet-printed thin-film transistor array manufactured on paper substrate for cheap electronic applications, Adv. Electron Mater. 3 (2017), https://doi.org/10.1002/aelm.201700275.
[2] H.N. Choi, S.H. Jee, J. Ko, D.J. Kim, S.H. Kim, Properties of surface heating textile for functional warm clothing based on a composite heating element with a positive temperature coefficient, Nanomaterials 11 (2021), https://doi.org/10.3390/nano11040904.
[3] G. Sathyanarayanan, M. Haapala, I. Kiiski, T. Sikanen, Digital microfluidic immobilized cytochrome P450 reactors with integrated inkjet-printed microheaters for droplet-based drug metabolism research, Anal. Bioanal. Chem. 410 (2018) 6677–6687, https://doi.org/10.1007/s00216-018-1280-7.
[4] H. Bartsch, D. Stöpel, J. Müller, A. Rydosz, European Microelectronics Packaging Conference Printed heater elements for smart sensor packages in LTCC, n.d. ⟨www.empc2017.pl⟩.
[5] Q. Zhou, A. Sussman, J. Chang, J. Dong, A. Zettl, W. Mickelson, Fast response integrated MEMS microheaters for ultra low power gas detection, Sens Actuators A Phys. 223 (2015) 67–75, https://doi.org/10.1016/j.sna.2014.12.005.
[6] M.S. Tolba, M. Fanni, G.A. Nasser, S. Umezu, A.M.R. Fath El-Bab, Design, Fabrication, and Control of Micro-Heater Based on Joule Effect for Low-Cost Medical Device, in: IECON Proceedings (Industrial Electronics Conference), IEEE Computer Society, 2022. https://doi.org/10.1109/IECON49645.2022.9969048.
[7] Y.K. Ryu, F. Carrascoso, R. López-Nebreda, N. Agraït, R. Frisenda, A. Castellanos-Gomez, Microheater actuators as a versatile platform for strain engineering in 2D materials, Nano Lett. 20 (2020) 5339–5345, https://doi.org/10.1021/acs.nanolett.0c01706.
[8] Y. Cao, J. Dong, High-performance low-voltage soft electrothermal actuator with directly printed micro-heater, Sens Actuators A Phys. 297 (2019), https://doi.org/10.1016/j.sna.2019.111546.
[9] S.L. Jia, H.Z. Geng, L. Wang, Y. Tian, C.X. Xu, P.P. Shi, Z.Z. Gu, X.S. Yuan, L.C. Jing, Z.Y. Guo, J. Kong, Carbon nanotube-based flexible electrothermal film heaters with a high heating rate, R. Soc. Open Sci. 5 (2018), https://doi.org/10.1098/rsos.172072.
[10] E. Jewell, B. Philip, P. Greenwood, Improved manufacturing performance of screen printed carbon electrodes through material formulation, Biosens. (Basel) 6 (2016), https://doi.org/10.3390/bios6030030.
[11] P.H. Wang, S.P. Chen, C.H. Su, Y.C. Liao, Direct printed silver nanowire thin film patterns for flexible transparent heaters with temperature gradients, RSC Adv. 5 (2015) 98412–98418, https://doi.org/10.1039/c5ra19804f.
[12] E.B. Secor, P.L. Prabhumirashi, K. Puntambekar, M.L. Geier, M.C. Hersam, Inkjet printing of high conductivity, flexible graphene patterns, J. Phys. Chem. Lett. 4 (2013) 1347–1351, https://doi.org/10.1021/jz400644c.
[13] D. Barmpakos, V. Belessi, R. Schelwald, G. Kaltsas, Evaluation of inkjet-printed reduced and functionalized water-dispersible graphene oxide and graphene on polymer substrate—Application to printed temperature sensors, Nanomaterials 11 (2021), https://doi.org/10.3390/nano11082025.
[14] A. Lee, K. Sudau, K.H. Ahn, S.J. Lee, N. Willenbacher, Optimization of experimental parameters to suppress nozzle clogging in inkjet printing, Ind. Eng. Chem. Res 51 (2012) 13195–13204, https://doi.org/10.1021/ie301403g.

[15] P. Serra, A. Piqué, Laser-Induced Forward Transfer: Fundamentals and Applications, Adv. Mater. Technol. 4 (2019) 1–33, https://doi.org/10.1002/admt.201800099.
[16] J. Bohandy, B.F. Kim, F.J. Adrian, Metal deposition from a supported metal film using an excimer laser, J. Appl. Phys. 60 (1986) 1538–1539, https://doi.org/10.1063/1.337287.
[17] P. Serra, M. Colina, J.M. Fernández-Pradas, L. Sevilla, J.L. Morenza, Preparation of functional DNA microarrays through laser-induced forward transfer, Appl. Phys. Lett. 85 (2004) 1639–1641, https://doi.org/10.1063/1.1787614.
[18] J.Marcos Fernández-Pradas, P. Serra, Laser-induced forward transfer: A method for printing functional inks, Cryst. (Basel) 10 (2020) 1–17, https://doi.org/10.3390/cryst10080651.
[19] J. Bohandy, B.F. Kim, F.J. Adrian, A.N. Jette, Metal deposition at 532 nm using a laser transfer technique, J. Appl. Phys. 63 (1988) 1158–1162, https://doi.org/10.1063/1.340023.
[20] A. Piqué, D. Chrisey, R. Auyeung, J. Fitz-Gerald, H. Wu, R. McGill, S. Lakeou, P. Wu, V. Nguyen, M. Duignan, A novel laser transfer process for direct writing of electronic and sensor material (1999) 279–284. https://doi.org/10.1007/s003399900306.
[21] M. Ali, E. Pages, A. Ducom, A. Fontaine, F. Guillemot, Controlling laser-induced jet formation for bioprinting mesenchymal stem cells with high viability and high resolution, Biofabrication 6 (2014), https://doi.org/10.1088/1758-5082/6/4/045001.
[22] M. Duocastella, J.M. Fernández-Pradas, J.L. Morenza, P. Serra, Sessile droplet formation in the laser-induced forward transfer of liquids: A time-resolved imaging study, Thin Solid Films 518 (2010) 5321–5325, https://doi.org/10.1016/j.tsf.2010.03.082.
[23] M. Duocastella, A. Patrascioiu, V. Dinca, J.M. Fernández-Pradas, J.L. Morenza, P. Serra, Study of liquid deposition during laser printing of liquids, in: Appl Surf Sci, Elsevier B.V., 2011: pp. 5255–5258. https://doi.org/10.1016/j.apsusc.2010.10.148.
[24] V. Dinca, M. Farsari, D. Kafetzopoulos, A. Popescu, M. Dinescu, C. Fotakis, Patterning parameters for biomolecules microarrays constructed with nanosecond and femtosecond UV lasers, Thin Solid Films 516 (2008) 6504–6511, https://doi.org/10.1016/j.tsf.2008.02.043.
[25] M. Gruene, C. Unger, L. Koch, A. Deiwick, B. Chichkov, Dispensing pico to nanolitre of a natural hydrogel by laser-assisted bioprinting, Biomed. Eng. Online 10 (2011), https://doi.org/10.1186/1475-925X-10-19.
[26] D. Munoz-Martin, C.F. Brasz, Y. Chen, M. Morales, C.B. Arnold, C. Molpeceres, Laser-induced forward transfer of high-viscosity silver pastes, Appl. Surf. Sci. 366 (2016) 389–396, https://doi.org/10.1016/j.apsusc.2016.01.029.
[27] T. Inui, R. Mandamparambil, T. Araki, R. Abbel, H. Koga, M. Nogi, K. Suganuma, Laser-induced forward transfer of high-viscosity silver precursor ink for non-contact printed electronics, RSC Adv. 5 (2015) 77942–77947, https://doi.org/10.1039/c5ra14119b.
[28] P. Sopeña, J. Sieiro, J.M. Fernández-Pradas, J.M. López-Villegas, P. Serra, Laser-induced forward transfer: a digital approach for printing devices on regular paper, Adv. Mater. Technol. 5 (2020), https://doi.org/10.1002/admt.202000080.
[29] H. Kim, R.C.Y. Auyeung, A. Piqué, Laser-printed thick-film electrodes for solid-state rechargeable Li-ion microbatteries, J. Power Sources 165 (2007) 413–419, https://doi.org/10.1016/j.jpowsour.2006.11.053.
[30] P. Sopeña, J.M. Fernández-Pradas, P. Serra, Laser-induced forward transfer of conductive screen-printing inks, Appl. Surf. Sci. 507 (2020), https://doi.org/10.1016/j.apsusc.2019.145047.
[31] D. Munoz-martin, Y. Chen, M. Morales, C. Molpeceres, Overlapping limitations for ps-pulsed lift printing of high viscosity metallic pastes, Met. (Basel) 10 (2020), https://doi.org/10.3390/met10020168.
[32] I. Theodorakos, A. Kalaitzis, M. Makrygianni, A. Hatziapostolou, A. Kabla, S. Melamed, F. de la Vega, I. Zergioti, Laser-induced forward transfer of high viscous, non-newtonian silver nanoparticle inks: jet dynamics and temporal evolution of the printed droplet study, Adv. Eng. Mater. 21 (2019), https://doi.org/10.1002/adem.201900605.
[33] M. Jalaal, M. Klein Schaarsberg, C.W. Visser, D. Lohse, Laser-induced forward transfer of viscoplastic fluids, J. Fluid Mech. 880 (2019) 497–513, https://doi.org/10.1017/jfm.2019.731.
[34] V. Dinca, A. Patrascioiu, J.M. Fernández-Pradas, J.L. Morenza, P. Serra, Influence of solution properties in the laser forward transfer of liquids, in: Appl Surf Sci, Elsevier B.V., 2012: pp. 9379–9384. https://doi.org/10.1016/j.apsusc.2012.02.007.
[35] A. Patrascioiu, C. Florian, J.M. Fernández-Pradas, J.L. Morenza, G. Hennig, P. Delaporte, P. Serra, Interaction between jets during laser-induced forward transfer, Appl. Phys. Lett. 105 (2014), https://doi.org/10.1063/1.4889802.
[36] W. Shen, X. Zhang, Q. Huang, Q. Xu, W. Song, Preparation of solid silver nanoparticles for inkjet printed flexible electronics with high conductivity, Nanoscale 6 (2014) 1622–1628, https://doi.org/10.1039/c3nr05479a.
[37] K. Dogome, T. Enomae, A. Isogai, Method for controlling surface energies of paper substrates to create paper-based printed electronics, Chem. Eng. Process.: Process. Intensif. 68 (2013) 21–25, https://doi.org/10.1016/j.cep.2013.01.003.
[38] C. Phillips, A. Al-Ahmadi, S.J. Potts, T. Claypole, D. Deganello, The effect of graphite and carbon black ratios on conductive ink performance, J. Mater. Sci. 52 (2017) 9520–9530, https://doi.org/10.1007/s10853-017-1114-6.